

D. BAUM, J. TITSCHACK

Cavity and Pore Segmentation in 3D Images with Ambient Occlusion

The manuscript will appear in a slightly different version in the EuroVis 2016 proceedings.

Zuse Institute Berlin
Takustrasse 7
D-14195 Berlin-Dahlem

Telefon: 030-84185-0
Telefax: 030-84185-125

e-mail: bibliothek@zib.de
URL: <http://www.zib.de>

ZIB-Report (Print) ISSN 1438-0064
ZIB-Report (Internet) ISSN 2192-7782

Cavity and Pore Segmentation in 3D Images with Ambient Occlusion

D. Baum¹ and J. Titschack^{2,3}

¹Zuse Institute Berlin (ZIB), Berlin, Germany

²MARUM - Center for Marine Environmental Sciences, Bremen, Germany

³Senckenberg am Meer, Wilhelmshaven, Germany

Abstract

Many natural objects contain pores and cavities that are filled with the same material that also surrounds the object. When such objects are imaged using, for example, computed tomography, the pores and cavities cannot be distinguished from the surrounding material by considering gray values and texture properties of the image. In this case, morphological operations are often used to fill the inner region. This is efficient, if the pore and cavity structures are small compared to the overall size of the object and if the object's shape is mainly convex. If this is not the case, the segmentation might be very difficult and may result in a lot of noise. We propose the usage of ambient occlusion for the segmentation of pores and cavities. One nice property of ambient occlusion is that it generates smooth scalar fields. Due to this smoothness property, a segmentation based on those fields will result in smooth boundaries at the pore and cavity openings. This is often desired, particularly when dealing with natural objects.

1 Introduction

Sedimentary rocks and biogenic materials, such as skeletons or shells, often exhibit specific cavities, pores and pore networks. A detailed geometric reconstruction of these void structures is a prerequisite for an improved rock classification and also serves for

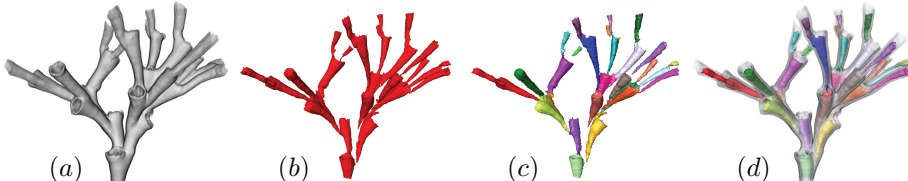


Figure 1: Cavity segmentation of a specimen of the scleractinian cold-water coral *Lophelia pertusa*. (a) Volume rendering of CT scan. (b) Segmented cavities. (c) Individual corallite cavities (calices) separated using hierarchical watershed on the average distance field computed using the ambient occlusion algorithm. (d) Semitransparent rendering of the corallites and the individual corallite cavities.

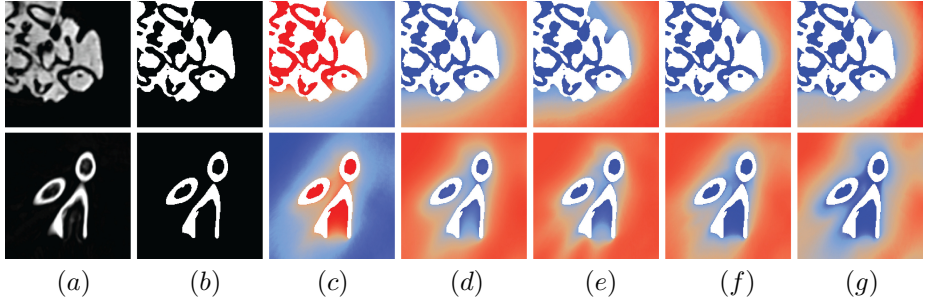


Figure 2: Results of ambient occlusion algorithm with 600 rays for a rock sample (top) and a coral (bottom). (a) Gray-scale image. (b) Binary image. The white voxels depict the foreground. Ambient occlusion was calculated on the background. (c) Ambient occlusion field. (d) Average distance field. (e) Eigenvalue field 1 (EV1). (f) EV2. (g) EV3. The colormap goes from blue (small value) to red (large values); picture edge length is 3.5 cm.

enhancing the understanding of porosity and permeability characteristics. In case of shells and skeletons, such as corals (see Fig. 1), the analysis of void structures provides important additional information for their morphological analysis and taxonomic classification [7, 12, 17, 20]. To date, these complex structures are commonly visualized with computed tomography [3, 28, 30], but their quantitative analysis is often hampered by the difficulty to discriminate cavities and pores from the sample surrounding region [23, 24]. Both regions have in common that they consist of the same matter (mostly air) so that in many cases their separation by gray values or texture properties is not feasible. Furthermore, the discrimination is often complicated by an irregular sample surface and a variable intrapore opening to the sample surface (see Fig. 3).

For datasets in which the cavities and pores have similar or equal values as the surrounding material, image segmentation tools like watershed [18], contour-based methods [11], or methods from discrete Morse theory [6, 9, 21] cannot be used. Furthermore, if the openings of the pores to the surrounding are wider than the pores themselves, distance field [10] approaches [8, 16] are also not applicable. In such cases, morphological operations [29] are often used, especially, for binary images. However, they often lead to a modification of the original outer shape, in particular if the shape exhibits a great irregularity or the size of the pores is large and varies strongly, thus resulting in a lot of noise.

In this paper, we propose the usage of ambient occlusion [4, 19, 32] for separating cavity and pore structures from the surrounding material. In molecular analysis, cavity extraction has been widely explored [13]. However, most of these techniques exploit the fact that molecules are approximated by atom spheres. The idea of using ambient occlusion for the distinction between inside and outside has previously been applied to molecular data for molecular path analysis by Lindow et al. [15]. We bring this idea further into the field of pore and cavity segmentation for binary images and present ambient occlusion as a simple and flexible method for this purpose. Fast ray traversal techniques are exploited for the efficient computation of the ambient occlusion field. We further enhance the idea of using ambient occlusion by providing additional feature fields that enable an improved classification of the cavity and pore structures. To show the applicability of the method, we present results for the segmentation of pores and cavities within a sedimentary rock and a coral.

2 Methods

As input to our method we assume a compact image domain $\mathcal{I} = \mathcal{B} \cup \mathcal{F} \subset \mathbb{R}^3$, consisting of background \mathcal{B} and foreground $\mathcal{F} = \mathcal{I} \setminus \mathcal{B}$, where \mathcal{I} is discretized into voxels. Furthermore, we assume that the cavities and pores to be extracted are part of \mathcal{B} and possibly are connected to the outside, which also belongs to \mathcal{B} . We build our method on top of mainly two previous works: the concept of ambient occlusion and a fast ray traversal.

2.1 Definition of ambient occlusion

For the definition of ambient occlusion, we follow the work by Correa and Ma [4], which not only considers a hemisphere, as is typically done, but all directions given by a full sphere \mathbf{S}^2 . Hence, we define ambient occlusion at position \mathbf{x} as

$$AO_\delta(\mathbf{x}) = \frac{1}{4\pi} \int_{\mathbf{S}^2} (1 - V_\delta(\mathbf{x}, \omega)) d\omega , \quad (1)$$

where the visibility at \mathbf{x} along direction ω is defined as

$$V_\delta(\mathbf{x}, \omega) = \begin{cases} 0 & , \text{ if } d_\delta(\mathbf{x}, \omega) < \delta \\ 1 & , \text{ else} \end{cases} .$$

Here, δ is a user-defined distance threshold and $d_\delta(\mathbf{x}, \omega)$ is the distance from a point $\mathbf{x} \in \mathcal{B}$ to the closest point $\mathbf{y} \in \mathcal{F}$ along direction ω . We differ from the work of Correa and Ma in two respects. First, we analyze binary images instead of scalar fields. Second, instead of sampling the image at regular intervals along the ray, we compute the ray's first intersection with the foreground.

2.2 Ray sampling and ray voxel traversal

Since we cannot evaluate Equation 1 analytically, we use a discrete approximation with a finite set of N rays only. Hence, we get

$$\overline{AO}_\delta(\mathbf{x}) = \frac{1}{N} \sum_{i=1}^N (1 - V_\delta(\mathbf{x}, \omega_i)) , \quad \omega_i \in \mathbf{S}^2 . \quad (2)$$

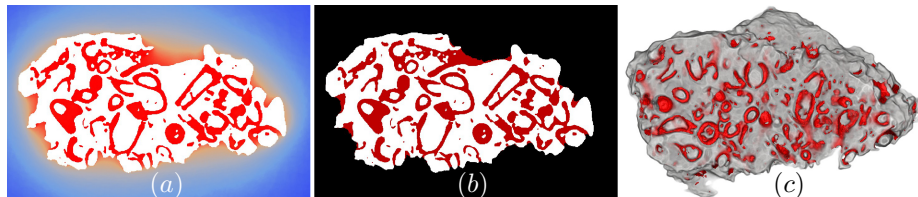


Figure 3: Cavity segmentation of a rock sample. White denotes the foreground. (a) AO field with colormap from blue (small) to red (large). (b) Threshold segmentation using AO field with threshold 0.84. (c) Cut through volume rendering and extracted cavities (red), highlighting that the cavities originate from the dissolution of corals and biogenic shells. Picture width is 11 cm.

The quality of this approximation depends on the number N of rays and the distribution of the ray directions. For a given N , a good sampling of directions can be obtained from a uniform sampling of points on S^2 , such as, for example, the method by Saff and Kuijlaars [25].

In order to efficiently evaluate Equation 2 for each background voxel, we need a fast ray traversal algorithm. Two ray traversal approaches were investigated closer. First, the classical ray traversal algorithm by Amanatides et al. [1] was implemented for both CPU and GPU. Second, we used the CPU-based approach by Revelles et al. [22] that combines the Amanatides algorithm with an octree-based approach.

2.3 Outputs of the algorithm

Our algorithm outputs several scalar fields. The first output is the ambient occlusion (AO) field itself, where each voxel is assigned the ambient occlusion value (Eq. 2) of the center point \mathbf{x} of the voxel. As second field we output the average distance (AD) of all rays to the foreground. In case the foreground is not hit by a ray, we can either ignore the ray or use δ as distance. In addition to these two fields, for each voxel we compute the covariance matrix Σ from the intersection points of the rays with the foreground. The eigenvalues (EV) of Σ give information about the variance of the intersection points w.r.t. the eigenvectors of Σ , which are the directions of main variation of the intersection points. For example, if the third eigenvalue is small, this means that the extension of the environment around this point is small in the direction of the third eigenvector. From the EV fields, further features can be derived such as standard anisotropy measures [2, 31]. Examples for AO, AD, and the EV fields are depicted in Figure 2.

2.4 Post processing

Background voxels that are adjacent to the foreground often exhibit considerably larger AO values than their neighbors, because many of the rays terminate already at their neighbors. These higher AO values cause noise on the outside surface of the object when using thresholding. In order to reduce these effects, we allow the user to identify such voxels and set their values to the average of the values of their 6-neighborhood. In the following, this operation will be called boundary filter.

3 Results

We tested the AO-based segmentation on CT scans of the scleractinian cold-water coral *Lophelia pertusa*, and a sedimentary rock sample from La Montagna, Sicily (Figs. 1-3). For both CT scans, a binary segmentation was generated using thresholding on the gray values, which served as input to our algorithm. All tests were performed on a system with 16 Intel(R) Xeon(R) CPU E5-2650 v2 @ 2.60GHz and an NVIDIA GeForce GTX 780 Ti graphics card with 3 GB of RAM.

Table 1: Performance of different ray traversal algorithms measured in seconds for the data sets of *Lophelia pertusa*, and a rock sample. The CPU versions were parallelized with OpenMP using different numbers of threads given in the table headings. The GPU version was implemented using OpenCL. Hyper-threading was used for running with 32 threads.

Coral	#Voxel	Foreground in %	Amanatides CPU¹				Octree CPU¹				Amanatides GPU²	
			1	8	16	32 ^h	1	8	16	32 ^h		
<i>L. pertusa</i>	272 × 150 × 295	1.8	6072	862	472	358	2390	437	350	259	34	
Rock sample	343 × 229 × 526	28.0	1745	250	140	111	1243	223	163	123	14	

¹System: 16 Intel(R) Xeon(R) CPU E5-2650 v2 @ 2.60GHz.

²Graphics: NVIDIA GeForce GTX 780 Ti with 3GB of RAM.

^h Using hyper-threading.

3.1 Performance

The running time of the AO algorithm depends on several factors: the size of the scan, the percentage of foreground voxels, the morphology of the pore and cavity space, the number of rays used to approximate AO, and the maximal length of the rays. In order to give a realistic estimate of the running time, we fixed the number of rays to 250. We found that this value is sufficiently high to produce smooth scalar fields. The parameter δ was set to the length of the image diagonal. With these settings, the Amanatides and octree ray traversal methods (see Sect. 2) were carried out on the GPU and CPU with different numbers of threads. The results are summarized in Table 1.

3.2 Cavity and Pore Segmentation

The two data sets were processed in the same way. First, we computed the AO field, followed by a correction of the AO values for voxels adjacent to the foreground using the boundary filter. Then thresholding was applied on the corrected AO field, where the threshold was determined interactively. The result for the coral *Lophelia pertusa* is shown in Figure 1(b). For the rock sample, Figure 3 presents the AO field together with a threshold segmentation. In Figure 3(b), it can be observed that the cavity segmentation at the pore openings smoothly follows the rock curvature.

3.3 Further Analysis

The coral data set was further processed in order to separate the individual corallite calices from one another, as shown in Figures 1 and 4 by the different colors. This is particularly interesting for taxonomic classification, since the calices differ in size and shape between species and morphotypes. To achieve this separation, we inverted the binary image of the pore space and compute the AD field for this inverted image, where only the pores and cavities belong to the background while the rest is foreground. In addition, we computed the 3D Euclidean distance map of the background. We then used hierarchical watershed on both the AD field and the 3D distance map to separate the calices. As can be seen in Figure 4, the separation based on the distance map (a) fails to produce satisfactory results (see regions encircled by ellipses) while the separation based on the AD field (b) provided a very good segmentation.

4 Discussion and Conclusion

As computed tomography becomes increasingly available to scientists, an effective cavity and pore segmentation might be of interest to various scientific disciplines, in particular the natural sciences. We have shown, that ambient occlusion (AO) represents a versatile tool for the separation of pore and cavity structures from interconnected surrounding regions. For the calculation of AO, we implemented and tested several algorithms for fast ray traversal. On the CPU, the octree ray traversal constitutes an improvement over the fast Amanatides ray traversal. However, the GPU version of the Amanatides algorithms, implemented with OpenCL, outperformed all other implementations, even those that were parallelized on the CPU. Thus, the natural extension to further speed-up the computation would be to test an octree ray traversal on the GPU, such as the sparse voxel octree [14].

We have shown that even simple thresholding on the computed scalar fields, especially the AO and AD fields, already allow for a good segmentation of pores and

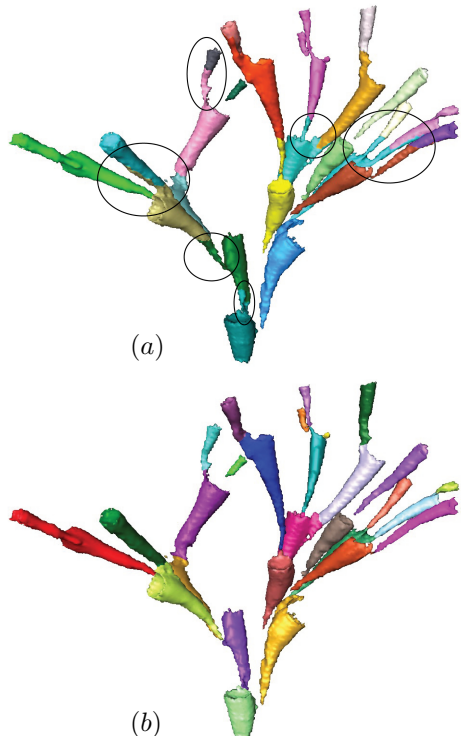


Figure 4: Corallite calice separation for *Lophelia pertusa* using hierarchical watershed on (a) the distance map, and (b) the average distance field computed with ambient occlusion. Some regions where the separation based on the distance map failed are highlighted with ellipses. Coral colony diameter is 9.5 cm.

cavities. By incorporating several scalar fields into the segmentation process, that is, AO, AD, EV and derived fields [2, 31], we expect further enhancements of the results. This can be done using supervised classification methods such as random forests [5]. Further improvements in the robustness of the segmentation might be achieved by running different methods with varying parameters and using boosting [26, 27] to generate a single segmentation.

For separating the pore structures into individual corallite calices, which is a prerequisite for taxonomic classification of the corals, we have used hierarchical watershed on the average distance field. Exploiting this feature for the separation significantly improved the results in comparison to the standard 3D distance map. We believe that this is due to the fact that the average distance is a statistical measure whereas the distance map only takes a single distance.

In summary, we have shown that ambient occlusion is a simple, easy to use, yet efficient and flexible tool that is well suited for the segmentation and analysis of cavity and pore structures. We believe that it is worthwhile to further investigate its capabilities, especially by considering several derived feature descriptors that can be computed with the help of ambient occlusion.

Acknowledgment

We thank A. Form (GEOMAR) and the BMBF project BIOACID II (FKZ 03F0655A) for providing the *L. pertusa* CT scan. Klinikum Bremen-Mitte, Prof. Dr. A.-J. Lemke and C. Timann are gratefully acknowledged for providing their facilities and performing the CT scans. We thank N. Lindow for providing the initial OpenCL code for the Amanatides ray traversal. C. Wienberg (MARUM) and the anonymous reviewers are thanked for their fruitful comments on the first version of this manuscript. JT was funded as GLOMAR associate scientists through DFG Research Center / Cluster of Excellence “The Ocean in the Earth System” and received additional funding by the DFG project Ti706/3-1 *Cold-water coral mound development underneath an eastern boundary upwelling system – the great wall off(f) Mauritania*.

References

- [1] John Amanatides, Andrew Woo, et al. A fast voxel traversal algorithm for ray tracing. In *Eurographics*, volume 87, page 10, 1987.
- [2] P.J. Basser and C. Pierpaoli. Microstructural and physiological features of tissues elucidated by quantitative-diffusion-tensor MRI. *Journal of Magnetic Resonance*, 111(3):209–219, June 1996.
- [3] Lydia Beuck, Agostina Vertino, Elizaveta Stepina, Marek Karolczak, and Olaf Pfannkuche. Skeletal response of *Lophelia pertusa* (Scleractinia) to bioeroding sponge infestation visualised with micro-computed tomography. *Facies*, 53(2):157–176, 2007.
- [4] Carlos D Correa and Kwan-Liu Ma. The occlusion spectrum for volume classification and visualization. *Visualization and Computer Graphics, IEEE Transactions on*, 15(6):1465–1472, 2009.

- [5] Antonio Criminisi and Jamie Shotton. *Decision forests for computer vision and medical image analysis*. Springer Science & Business Media, 2013.
- [6] Olaf Delgado-Friedrichs, Vanessa Robins, and Adrian Sheppard. Skeletonization and partitioning of digital images using discrete Morse theory. *Pattern Analysis and Machine Intelligence, IEEE Transactions on*, 37(3):654–666, 2015.
- [7] Claudia Färber, Jürgen Titschack, Christine H. L. Schönberg, Karsten Ehrig, Karin Boos, Daniel Baum, Bernd Illerhaus, Ulla Asgaard, Richard G. Bromley, André Freiwald, and Max Wissak. Long-term macrobioerosion in the mediterranean sea assessed by micro-computed tomography. *Biogeosciences Discussions*, 2016.
- [8] Ali M Ghalib and Roman D Hryciw. Soil particle size distribution by mosaic imaging and watershed analysis. *Journal of Computing in Civil Engineering*, 13(2):80–87, 1999.
- [9] Attila Gyulassy, David Günther, Joshua A Levine, Julien Tierny, and Valerio Pasucci. Conforming Morse-Smale complexes. *Visualization and Computer Graphics, IEEE Transactions on*, 20(12):2595–2603, 2014.
- [10] Mark W Jones, Jakob Andreas Bærentzen, and Milos Srivastava. 3d distance fields: A survey of techniques and applications. *Visualization and Computer Graphics, IEEE Transactions on*, 12(4):581–599, 2006.
- [11] Michael Kass, Andrew Witkin, and Demetri Terzopoulos. Snakes: Active contour models. *International journal of computer vision*, 1(4):321–331, 1988.
- [12] Mark A Knackstedt, Robert M Sok, Adrian P Sheppard, Shane J Latham, Mahyar Madadi, Trond Varslot, Christoph H Arns, Gregor Bachle, Gregor Eberli, et al. Probing pore systems in carbonates: correlations to petrophysical properties. In *49th Annual Logging Symposium*. Society of Petrophysicists and Well-Log Analysts, 2008.
- [13] Michael Krone, Barbora Kozlikova, Norbert Lindow, Marc Baaden, Daniel Baum, Julius Parulek, Hans-Christian Hege, and Ivan Viola. Visual analysis of biomolecular cavities: State of the art. 2016. Submitted to EuroVis 2016 STARS, conditionally accepted.
- [14] Samuli Laine and Tero Karras. Efficient sparse voxel octrees. *Visualization and Computer Graphics, IEEE Transactions on*, 17(8):1048–1059, 2011.
- [15] Norbert Lindow, Daniel Baum, and Hans-Christian Hege. Voronoi-based extraction and visualization of molecular paths. *Visualization and Computer Graphics, IEEE Transactions on*, 17(12):2025–2034, 2011.
- [16] Norberto Malpica, Carlos Ortiz de Solorzano, Juan José Vaquero, Andrés Santos, Isabel Vallcorba, Jose Miguel García-Sagredo, and Francisco del Pozo. Applying watershed algorithms to the segmentation of clustered nuclei. *Cytometry*, 28:289–297, 1997.
- [17] Kei Matsuyama, Jürgen Titschack, Daniel Baum, and André Freiwald. Two new species of erect *Bryozoa* (Gymnolaemata: Cheilostomata) and the application of non-destructive imaging methods for quantitative taxonomy. *Zootaxa*, 4020(1):81, 2015.

- [18] Fernand Meyer. Topographic distance and watershed lines. *Signal processing*, 38(1):113–125, 1994.
- [19] Gavin Miller. Efficient algorithms for local and global accessibility shading. In *Proceedings of the 21st annual conference on Computer graphics and interactive techniques*, pages 319–326. ACM, 1994.
- [20] A. Morales Pinzón, M. Orkisz, C. M. Rodríguez Useche, J. S. Torres González, S. Teillaud, J. A. Sánchez, and M. Hernández Hoyos. A semi-automatic method to extract canal pathways in 3d micro-ct images of octocorals. *PLoS ONE*, January 2014.
- [21] J Reininghaus, D Günther, I Hotz, T Weinkauf, and HP Seidel. Combinatorial gradient fields for 2d images with empirically convergent separatrices, 2012. *arXiv preprint Arxiv:1208.6523*.
- [22] J. Revelles, C. Ureña, and M. Lastra. An efficient parametric algorithm for octree traversal. In *Journal of WSCG*, pages 212–219, 2000.
- [23] RC Roche, RL Abel, KG Johnson, and CT Perry. Spatial variation in porosity and skeletal element characteristics in apical tips of the branching coral *Acropora pulchra* (Brook 1891). *Coral reefs*, 30(1):195–201, 2011.
- [24] Ronan C Roche, Richard A Abel, Kenneth G Johnson, and Chris T Perry. Quantification of porosity in *Acropora pulchra* (Brook 1891) using x-ray micro-computed tomography techniques. *Journal of Experimental Marine Biology and Ecology*, 396(1):1–9, 2010.
- [25] Edward B Saff and A BJ Kuijlaars. Distributing many points on a sphere. *The mathematical intelligencer*, 19(1):5–11, 1997.
- [26] Robert E Schapire. The strength of weak learnability. *Machine learning*, 5(2):197–227, 1990.
- [27] Florian Schroff, Antonio Criminisi, and Andrew Zisserman. Object class segmentation using random forests. In *BMVC*, pages 1–10, 2008.
- [28] Asuka Sentoku, Hitomi Morisaki, Shinji Masumoto, Rie Ohno, Takayuki Tomiyama, and Yoichi Ezaki. Internal skeletal analysis of the colonial azooxanthellate scleractinian *Dendrophyllia cribrosa* using microfocus x-ray CT images: Underlying basis for its rigid and highly adaptive colony structure. *Journal of structural biology*, 189(1):37–43, 2015.
- [29] Pierre Soille. *Morphological image analysis: principles and applications*. Springer Science & Business Media, 2013.
- [30] LA Viskova and AV Pakhnevich. A new boring bryozoan from the Middle Jurassic of the Moscow region and its micro-CT research. *Paleontological Journal*, 44(2):157–167, 2010.
- [31] C.-F. Westin, S. Peled, H. Gudbjartsson, R. Kikinis, and F. A. Jolesz. Geometrical diffusion measures for MRI from tensor basis analysis. In *ISMRM '97*, page 1742, Vancouver Canada, April 1997.
- [32] Sergey Zhukov, Andrei Iones, and Grigorij Kronin. An ambient light illumination model. In *Rendering Techniques '98*, pages 45–55. Springer, 1998.